

Parametric study of the small scale linear Fresnel reflector



A. Barbón^a, N. Barbón^a, L. Bayón^{b,*}, J.A. Sánchez-Rodríguez^a

^a Department of Electrical Engineering, University of Oviedo, Campus of Gijón, Spain

^b Department of Mathematics, University of Oviedo, Campus of Gijón, Spain

ARTICLE INFO

Article history:

Received 23 January 2017

Received in revised form

20 July 2017

Accepted 20 September 2017

Available online 22 September 2017

Keywords:

Linear fresnel reflector

Parametric study

Sensitivity analysis

ABSTRACT

This paper addresses the influence of the transversal and longitudinal parameters in the performance of a small scale linear Fresnel reflector (SSLFR) without longitudinal movement. The main purpose of this study is to show the influence of the design parameters (receiver height, mirror length, and mirror width) on the energy absorbed by the absorber tube. In addition, the influence of these parameters on the shading of the absorber tube is also analysed. Different configurations are analysed regarding the longitudinal angle that the mirrors and the absorber tube form with the horizontal plane. Each of these configurations is analysed considering the optimal length and longitudinal position of the absorber tube. Numerical simulations show the influence of mirror width, mirror length, and receiver height on the energy absorbed. The simulations allow us to analyze the monthly variation of this influence throughout the year, considering also the effect of the latitude. A sensitivity analysis is also carried out in order to evaluate the importance of the parameters.

© 2017 Elsevier Ltd. All rights reserved.

1. Introduction

Linear Fresnel Reflectors (LFRs) are becoming an option to generate electricity from solar radiation, although almost all recent Solar Thermal Power Plants are parabolic trough plants. Apart from prototypes, there are several commercial LFR plants for power generation: Kimberlina Solar Thermal Power Plant (see Ref. [25] (5 MW) in California, (USA); Liddell Power Station's solar boiler (9.3 MW) in Australia; Puerto Errado 2 (30 MW) in Spain; and Dhursar (125 MW) in India. LFR plants are built using two different configurations (see Refs. [3] and [21]: the central LFR, where the receiver is in the center of the mirror array; and the compact linear Fresnel collector (CLFC) [19], where there is a receiver at each side of the mirror array so that consecutive mirrors point to a different receiver. The main advantage of the CLFC configuration against the central LFR is that blocking optical losses are smaller, since consecutive mirrors point to a different receiver depending on the incidence angle. Furthermore, several authors have studied the different characteristics of both configurations (see, for example, [1,2,16,23]; or [26], namely: receiver design (multiple tube receiver or single-tube receiver), mirror construction (curved or flat), and secondary concentrator design (with or without secondary

concentrator). Particularly, Kimberlina is a CLFC plant, with a multi-tube receiver and without a secondary concentrator; Liddell and Dhursar are CLFC plants, whereas Puerto Errado is a LFR plant, with a single-tube absorber and with a secondary concentrator.

LFR technology can be used in other applications, besides electricity generation, as in industrial processes and in the building sector. For example, these collectors can be used in domestic water heating [30] and [31], in an absorption air cooled Solar-GAX cycle [33], or to provide heating/cooling for buildings [7]. These applications are not negligible, since in the European Union (EU) the building sector is one of the highest energy consumers, in particular it represents more than 40% of the final energy consumption (see Ref. [14]). In order to improve energy efficiency, the EU [13] has adopted a series of directives to promote the use of energy from renewable sources in buildings.

Numerous authors have made parametric studies of this technology for electricity generation (see, for example, [4,9,24]; or [2], although the longitudinal design has been overlooked in most of these studies. In contrast, there are only a few parametric studies of LFRs in other applications (see Barbón et al. [5,6] and [6]. In large scale LFRs the study of the longitudinal behaviour is not usually performed for two reasons: the absorber size does not permit any configuration allowing the modification of its position, and the influence of the longitudinal position can be considered irrelevant in % terms with respect to the total length of the absorber. However, in small scale LFRs (SSLFRs) this is a

* Corresponding author.

E-mail address: bayon@uniovi.es (L. Bayón).

| Nomenclature | | | |
|--------------|--|--------------|---|
| A | Longitudinal component of the reflected radiation | M_{fw} | Mirror Field Width (m) |
| A_{eff} | Effective area of the absorber tube (m^2) | N | Number of mirrors at each side of the central mirror |
| A_{fw} | Mirror Field Area (m^2) | Q | Total power absorbed (W) |
| B_i | Transversal component of the reflected radiation for $i - th$ mirror ($0 \leq i \leq n$) | S_t | Transversal shading of the absorber tube (m) |
| CL_g | Cleanliness factor of the glass | W | Width of the mirrors (m) |
| CL_m | Cleanliness factor of the mirror | W_{ai} | Width illuminated on the absorber by the i -th by mirror (m) |
| D | Diameter of the absorber tube (m) | α | Absorptivity of the absorber tube |
| DNI | Direct Normal Irradiance (W/m^2) | α_i | Angle between the vertical at the focal point and the line connecting the center point of each mirror to the focal point ($^\circ$) |
| d | Separation between two consecutive mirrors (m) | α_S | Height angle of the Sun ($^\circ$) |
| f | Height of the receiver (m) | β_a | Angle between the absorber tube and the horizontal plane ($^\circ$) |
| IAF | Incidence angle modifier | β_i | Tilt of $i - th$ mirror ($^\circ$) |
| L_{abs} | Length of the single absorber tube (m) | β_M | Angle between the mirror axis and the horizontal plane ($^\circ$) |
| L_{abs}^l | Left length of the single absorber tube (m) | γ_S | Azimuth of the sun ($^\circ$) |
| L_{abs}^r | Right length of the single absorber tube (m) | η_{opt} | Optical efficiency (%) |
| L_{abs} | Total illuminated length of the single absorber tube (m) | θ_i | Angle between the normal to the mirror and the angle of incidence of the sun ($^\circ$) |
| L_{ai} | Length of the circumference illuminated on the absorber by the $i - th$ mirror (m) | θ_L | Lateral incidence angle ($^\circ$) |
| L_i | Position of $i - th$ mirror ($0 \leq i \leq n$) (m) | θ_l | Longitudinal incidence angle ($^\circ$) |
| L_i^l | L_i of the left side (m) | θ_t | Transversal incidence angle ($^\circ$) |
| L_i^r | L_i of the right side (m) | θ_z | Zenith angle of the Sun ($^\circ$) |
| L_M | Length of the mirrors (m) | λ | Latitude angle ($^\circ$) |
| L_{ts} | Position of transversal shading of the absorber tube (m) | μ | Angle between the reflected ray and the normal to the NS axis ($^\circ$) |
| l_{abs}^l | Left illuminated length of the single absorber tube (m) | ρ | Reflectivity of the primary mirrors |
| l_{abs}^r | Right illuminated length of the single absorber tube (m) | τ | Transmissivity of the glass |

fundamental study. Another parameter that affects the study of SSLFRs is the area available for installation. In large scale LFRs, the available area is not a critical parameter. In contrast, the mirror field area (A_{fw}) is the starting parameter for the design of a SSLFR. As already mentioned, these SSLFRs can be used in domestic water heating, or to provide heating/cooling for buildings. Therefore, roofs are a logical location for the SSLFR. The installation on building roofs reduces the risk of shading by adjacent buildings, vegetation, or other sources of shadow. However, the roofs of the urban buildings are generally not designed or built to host renewable energy systems. Available roof area has in fact been identified as a main limiting factor in achieving zero energy buildings, especially for taller buildings.

The potential number of SSLFRs to be installed on a roof strongly depends on the mirror field area. And, as we will see in Section 2, this parameter can be expressed in terms of the mirror length, receiver height, and mirror width. Therefore, one of the objectives of this study is to analyze the influence of the variation of these parameters, in a reasonable range, on the energy absorbed by the absorber tube, and, as a consequence, on the potential energy that can be obtained in a particular roof. Another objective is to analyze the influence of these parameters on the shading of the absorber tube on the mirror field area.

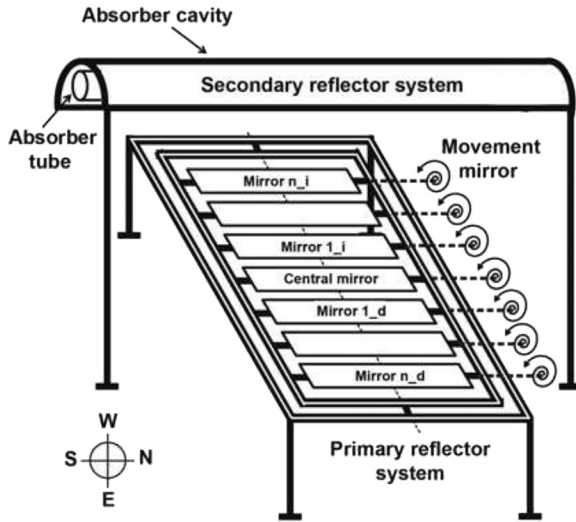
The paper is organized as follows. Section 2 summarizes the main angular relationships that will be used throughout the paper, the parameters used in the transversal study, the parameters used in the longitudinal study, and the equation used to determine the power absorbed by the absorber tube. In Section 3 (critical parameters), the parameters used in the comparative analysis are

presented. In addition, an evaluation of the shading effect of the absorber tube is carried out. Numerical simulations and sensitivity analysis are presented in Section 4 for different configurations of the LFR. Finally, Section 5 summarizes the main contributions and conclusions of the paper.

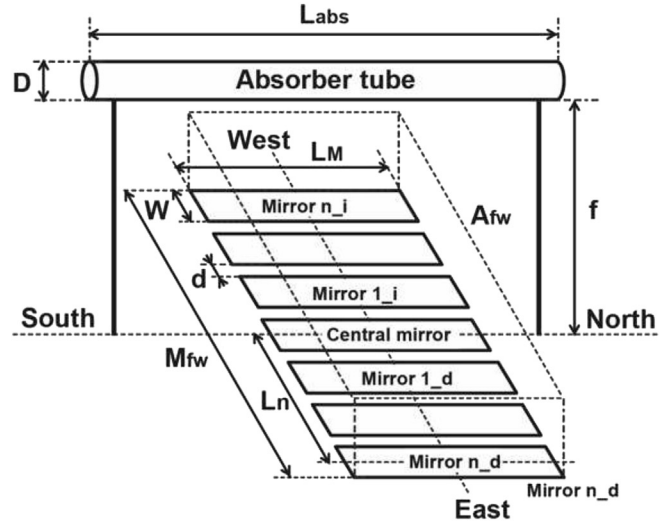
2. Problem statement and definitions

The SSLFR, as shown in Fig. 1a, is composed of two main blocks: the primary reflector system and the secondary reflector system. The primary reflector system is composed of a fixed frame with rows of mirrors. The secondary reflector system consists of an absorber tube and an absorber cavity. The secondary reflector system is located at a certain height from the primary reflector system. Each row of mirrors tracks the sun on one axis (East-West axis tracking). The assumptions made in this study are as follows:

- (i) The mirrors are flat and specularly reflecting.
- (ii) The rows of mirrors are perfectly tracked so as to follow the apparent movement of the Sun.
- (iii) The pivoting point of each mirror coincides with the central point of the mirror; hence, it is always focused on the central point of the absorber tube.
- (iv) An appropriate distance (shift) must be kept between two consecutive mirrors so that a mirror does not shade its adjacent mirror element.
- (v) A single absorber tube is used.
- (vi) The design of the absorber tube and the absorber cavity will not be taken into consideration.



(a) Schematic of a SSLFR.



(b) Parameters.

Fig. 1. The SSLFR.

2.1. Angular relationships

Considering a SSLFR aligned horizontally and aligned in a North-South orientation, the angle of incidence of solar radiation will be calculated in two projection planes: the transversal incidence angle (θ_t) and the longitudinal incidence angle (θ_l), (see Ref. [32]. The transversal incidence angle (θ_t) is defined as the angle between the vertical and the projection of the sun vector on the East-West plane (the plane orthogonal to the absorber tube), and the longitudinal incidence angle (θ_l) is defined as the angle between the vertical and the projection of the sun vector on the North-South plane.

2.2. Parameters used in the transversal study

As shown in Barbon et al., [5,6]; each mirror can be characterized by two parameters: position with respect to the central mirror (L_i), and tilt (β_i). The position (L_i) depends on the mirror width (W) and the mirror separation (d). The tilt (β_i) depends on the receiver height (f), the diameter of the absorber tube (D), and the transversal incidence angle (θ_t). If n is the number of mirrors at each side of the central mirror, the total number of mirrors of the SSLFR is $2n + 1$.

The illuminated width on the absorber tube by the i -th mirror (W_{ai}) is given by:

$$W_{ai} = W[\cos\beta_i \pm \sin\beta_i \tan\alpha_i]; \quad 0 \leq i \leq 2n \quad (1)$$

where α_i is the angle between the vertical at the focal point and the line connecting the center point of each mirror to the focal point. The sign \pm must be adopted according to the following criteria: – for the left side, and + for the right side. The angle α_i can be calculated as:

$$\alpha_i = \arctan\left[\frac{i \cdot (W + d)}{f + D/2}\right]; \quad 1 \leq i \leq n \quad (2)$$

The length of the circumference illuminated on the absorber tube (L_{ai}) by the i -th mirror for $0 \leq i \leq 2n$, can be calculated as:

$$L_{ai} = \begin{cases} \frac{\pi D}{2} & \text{if } W_{ai} \cos\alpha_i > D \\ D \arcsin\left(\frac{W_{ai}}{D}\right) & \text{if } W_{ai} \cos\alpha_i \leq D \end{cases} \quad (3)$$

2.3. Parameters used in the longitudinal study

As shown in Barbon et al., [5,6]; the parameters used in the longitudinal study are as follows: angle between the mirror axis and the horizontal plane (β_M), angle between the absorber tube and the horizontal plane (β_a), zenithal solar angle (θ_z), mirror length (L_M), distance between the absorber and the mirror (f), angle between the reflected beam and the zenith (μ), and angle between the incident ray and the normal plane to the mirror (θ_L). These parameters allow the calculation of the left illuminated length of the absorber (l_{abs}^l), the right illuminated length of the absorber (l_{abs}^r), and the total illuminated length of the single absorber tube (l_{abs}).

2.4. Mirror field area

The parameters that influence the installation of SSLFRs on building roofs are of two types: those intrinsic to the SSLFR and those relating to the roof. The potential number of SSLFRs to be installed on a roof strongly depends on these parameters. Fig. 1 b shows the area required for the installation of a SSLFR, that is, the mirror field area (A_{fw}), which is given by:

$$A_{fw} = L_M \cdot [2n(W + d) + W] \quad (4)$$

2.5. Power absorbed

Different equations are used in the literature to determine the power absorbed by the absorber tube of a LFR (see, for example

[12,22], and [10]. We will use a version of these equations presented by Ref. [6]; that it is particularly suitable for the case of SSLFRs:

$$Q = \sum_{i=0}^{2 \cdot n} DNI \cdot \eta_{opt} \cdot IAF_i \cdot A_{effi} \quad (5)$$

where these parameters are:

- (i) DNI is the direct normal irradiance.
- (ii) η_{opt} is the total optical yield, which is calculated considering the reflectivity of the mirrors (ρ), the cleanliness factors of the mirror (CI_m) and of the glass covering the secondary absorber (CI_g), the transmissivity of this glass (τ), and the absorptivity of the material of which the absorber tube is made (α). Although some of these parameters, especially τ , should change with the angle of incidence (see Ref. [11], in this study they are considered constant for simplicity (see Binotti et al. [8], Moghumi et al. [20]. These values are: $\rho = 0.94$ (see Ref. [11]; $CI_m = CI_g = 0.96$ (see Ref. [28]; $\tau = 0.87$ if $\alpha_i \leq 20^\circ$, $\tau = 0.85$ if $20^\circ \leq \alpha_i \leq 30^\circ$ (see Ref. [32].
- (iii) IAF_i considers the variation in the optical performance of a SSLFR for varying ray incidence angles, by the i -th mirror:

$$IAF_i = \left[A^2 + B_i^2 + 2 \cdot A \cdot B_i \cdot \cos \widehat{AB}_i \right]^{1/2}; \quad 0 \leq i \leq 2n \quad (6)$$

where A (common to all the mirrors) and B_i (different for each mirror) are the components of the reflected radiation, and their values are given by:

$$A = \cos \gamma_S \cdot \cos \theta_L; \quad B_i = \frac{\cos \alpha_S \cdot \sin \gamma_S \cdot \cos \theta_i}{\sin \theta_t}; \quad 0 \leq i \leq 2n \quad (7)$$

Fig. 2 shows the components of the reflected radiation (A and B_i).

- (iv) A_{effi} is the effective area of the absorber tube by the i -th mirror that is actually illuminated, which is calculated considering the length of the circumference illuminated on the absorber tube by the i -th mirror (L_{ai}), and the total illuminated length of the absorber tube (l_{abs}):

$$A_{effi} = L_{ai} \cdot l_{abs}; \quad 0 \leq i \leq 2n \quad (8)$$

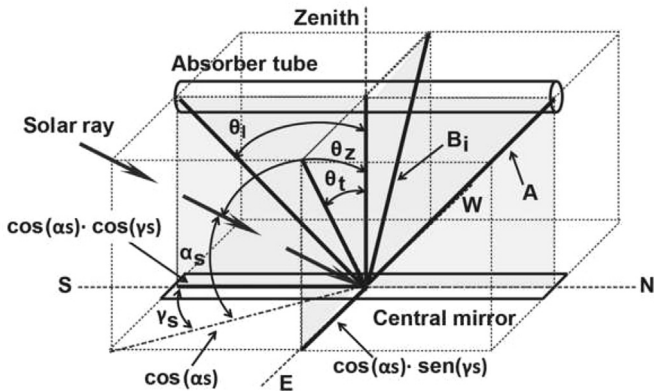


Fig. 2. Components of the reflected radiation.

3. Parameters object of study

In this study, the mirrors and the absorber tube are not provided with longitudinal movement. We will study 4 different configurations for the relative position between the field of primary mirrors, the absorber tube and the horizontal plane.

Table 1 shows these 4 configurations. C_1 is the configuration used in large-scale LFRs, where the mirrors and the absorber tube form an angle of 0° with the horizontal plane. This configuration will be used as a basis for the sake of comparison with the others. Configuration C_2 , has an angle of inclination of the mirrors equal to the latitude, with the absorber tube remaining in the horizontal position. In configuration C_3 , both mirrors and absorber tube have an inclination equal to the latitude. In configuration C_4 the mirrors form an angle of 0° with the horizontal plane and the absorber tube has an inclination equal to minus the latitude. The configurations that imply inclining the entire mirror row and/or inclining the entire absorber tube seem to work only for SSLFRs, since it would be unrealistic to incline large-scale LFRs.

The tilt angle is chosen equal to the site latitude, as in the so-called single axis polar solar tracker, which sometimes add a correction as a function of the declination. With this arrangement, the rotation axis of the mirror, oriented in the N-S direction, is parallel to the Earth's axis. Compared to two axes systems, single axis systems are reported to reach yields of 96%.

3.1. Critical parameters

In large scale LFRs, the optimization of the longitudinal position and length of the absorber tube is not considered. However, in a SSLFR this longitudinal optimization is essential, that is, the longitudinal position and length of the absorber tube are critical parameters for the study of a SSLFR. The longitudinal optimization involves the calculation of the optimal values of the total length, left length, and right length of the absorber tube (L_{abs} , L_{abs}^L , and L_{abs}^R respectively).

As can be seen in Barbón et al. [6]; the longitudinal position and length of the absorber tube are two critical parameters for the design of a SSLFR. Using non-optimal values leads to decreases of up to 80% in the energy produced.

This comparative analysis uses the optimal values of L_{abs} , L_{abs}^L , and L_{abs}^R . In Ref. [6] a new mathematical algorithm that allows the optimization of the position and length of the absorber tube based on the longitudinal design is presented. The method is based on a geometrical algorithm that minimizes the area between two curves, minimizing the end loss and reflected light loss, which are now taken into consideration. Table 2 summarizes these values for $f = 1.5$ (m) and $L_M = 2$ (m), in Almeria (Spain), with latitude $36^\circ 50' 07'' N$, longitude $02^\circ 24' 08'' W$ and Berlin (Germany), with latitude $52^\circ 31' 7'' N$, longitude $13^\circ 24' 37'' E$.

With the sign convention that we have adopted, lengths from the center of the mirror to the left are considered positive, and those to the right, negative.

Table 1
Characteristics of each configuration.

| Configuration | Mirrors | Absorber |
|---------------|------------------------|------------------------|
| | β_M ($^\circ$) | β_a ($^\circ$) |
| C_1 | 0 | 0 |
| C_2 | λ | 0 |
| C_3 | λ | λ |
| C_4 | 0 | $-\lambda$ |

Table 2
Optimization of the length and position of the absorber tube.

| Configuration | Almeria | | | Berlin | | |
|----------------|-------------|-------------|-----------|-------------|-------------|-----------|
| | L_{abs}^l | L_{abs}^r | L_{abs} | L_{abs}^l | L_{abs}^r | L_{abs} |
| C ₁ | -0.425 | -2.425 | 2.00 | -0.865 | -2.865 | 2.00 |
| C ₂ | 2.807 | 0.047 | 2.76 | 3.862 | 0.393 | 3.468 |
| C ₃ | 2.029 | 0.029 | 2.00 | 2.190 | 0.190 | 2.00 |
| C ₄ | -0.300 | -1.756 | 1.456 | -0.581 | -1.798 | 1.217 |

3.2. Parameters used in the comparative analysis

The following parameters remain constant in all the configurations:

- (i) $n = 12$, considered optimal for the design of a SSLFR.
- (ii) $D = 0.0486$ (m), considered appropriate in the manufacture of the prototype, since the absorber tube is manufactured from standardized carbon steel tubes (UNE EN 10255). This diameter is the standardized value that best conforms to the dimensions of the prototype that is being built.
- (iii) L_{abs} , L_{abs}^l , and L_{abs}^r , see Table 2.
- (iv) $d = 0.024$ (m), this value is used by Barbon et al. [5,6]; where the authors use a method inspired by what is known as 'Mathur's method' [17] and [18], which calculates the appropriate value of the shift between adjacent mirrors such that shading and blocking of reflected rays are avoided. Using this method, the effects of shading and blocking are avoided, for a transversal incidence angle between -22.5° and 22.5° . In any case, the numerical simulations, performed using MATLAB, also take into account the effects of shading and blocking, in those hours in which they exist.

The comparative analysis is performed changing parameter values around the following values, considered as basic dimensions (D_B):

- (i) $f = 1.5$ (m), considered optimal for the design of a SSLFR and obtained by applying Mathur's method.
- (ii) $L_M = 2$ (m), considered optimal for the design of a SSLFR and obtained by applying Mathur's method.
- (iii) $W = 0.060$ (m), considered optimal for the design of a SSLFR.

Table 3 summarizes the parameter values selected for the analysis in each configuration. These values are expressed in percentage terms of the basic dimensions.

3.3. Evaluation of the shading of the absorber tube

Fig. 3 shows the most the transversal shading of the absorber tube. The transversal shading of the absorber tube can be determined using the following equation:

Table 3
Geometrical parameters of the selected configurations.

| Parameters | % D_B | | | | |
|------------|----------------|----------------|----------------|----------------|----------------|
| | D ₁ | D ₂ | D ₃ | D ₄ | D ₅ |
| f | 70 | 85 | 100 | 115 | 130 |
| L_M | 70 | 85 | 100 | 115 | 130 |
| W | 70 | 85 | 100 | 115 | 130 |

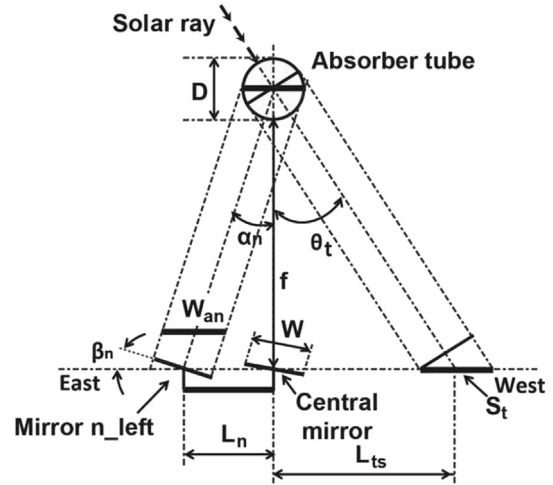


Fig. 3. Transversal shading of the absorber tube.

$$S_t = \frac{D}{\cos\theta_t} \quad (9)$$

where S_t is the transversal shading of the absorber tube (m). According to Fig. 3 is met:

$$L_{ts} = \left(f + \frac{D}{2}\right) \cdot \tan\theta_t \quad (10)$$

where L_{ts} is the position of the transversal shading of the absorber tube (m).

$$L_i = i \cdot (W + d); \quad 0 \leq i \leq 2n \quad (11)$$

where L_i is the position of i -th mirror ($0 \leq i \leq n$) (m). There is no transversal shading if:

$$\left(L_{ts} + \frac{S_t}{2}\right) - \left(L_i + \frac{W_{ai}}{2}\right) > S_t; \quad 0 \leq i \leq 2n \quad (12)$$

or

$$\left(L_i + \frac{W_{ai}}{2}\right) - \left(L_{ts} + \frac{S_t}{2}\right) > W_{ai}; \quad 0 \leq i \leq 2n \quad (13)$$

4. Results and discussion

Regardless of the application where the SSLFR will be used (domestic water heating or heating/cooling for buildings), the thermal behaviour is not the only concern. As SSLFRs are usually installed on building roofs, the mirror field area, given by the parameters M_{fw} and L_M , has to be carefully considered.

All the calculations are based on sub-hourly distribution of direct normal irradiance in a specific geographic location: Almeria (Spain), with latitude $36^\circ 50' 07'' N$, longitude $02^\circ 24' 08'' W$ and altitude 22 m and Berlin (Germany), with latitude $52^\circ 31' 7'' N$, longitude $13^\circ 24' 37'' E$ and altitude 37 m. Derived database and system integrating data [27] have been used to estimate the solar irradiance. Numerical simulations were performed using the computational software package MATLAB. The program developed incorporates subroutines, discretized every 10 min, to calculate: DNI, mirror position, IAF, L_{ai} , and l_{abs} . The program takes into

Table 4
Energy absorbed by the absorber tube (MWh).

| | Alm | Ber | Alm | Ber | Alm | Ber | Alm | Ber |
|----|-----------|------|----------|------|----------|------|----------|------|
| | January | | February | | March | | April | |
| C1 | 0.39 | 0.11 | 0.47 | 0.19 | 0.74 | 0.33 | 0.81 | 0.51 |
| C2 | 0.37 | 0.21 | 0.46 | 0.33 | 0.75 | 0.54 | 0.84 | 0.79 |
| C3 | 0.38 | 0.21 | 0.47 | 0.32 | 0.73 | 0.46 | 0.77 | 0.60 |
| C4 | 0.31 | 0.06 | 0.38 | 0.12 | 0.59 | 0.20 | 0.66 | 0.31 |
| | May | | June | | July | | August | |
| C1 | 0.90 | 0.70 | 0.93 | 0.64 | 0.96 | 0.70 | 0.91 | 0.61 |
| C2 | 0.97 | 1.08 | 1.05 | 1.00 | 1.06 | 1.09 | 0.96 | 0.94 |
| C3 | 0.87 | 0.75 | 0.91 | 0.67 | 0.94 | 0.74 | 0.87 | 0.68 |
| C4 | 0.77 | 0.43 | 0.81 | 0.39 | 0.83 | 0.43 | 0.76 | 0.37 |
| | September | | October | | November | | December | |
| C1 | 0.73 | 0.40 | 0.59 | 0.26 | 0.41 | 0.13 | 0.36 | 0.08 |
| C2 | 0.75 | 0.64 | 0.58 | 0.43 | 0.39 | 0.24 | 0.34 | 0.17 |
| C3 | 0.71 | 0.51 | 0.58 | 0.40 | 0.40 | 0.24 | 0.35 | 0.17 |
| C4 | 0.59 | 0.24 | 0.47 | 0.16 | 0.33 | 0.08 | 0.29 | 0.05 |

account the effects of shading, blocking and end loss.

4.1. Influence of the parameters on the energy absorbed by the absorber tube

Table 4 shows the energy absorbed by the absorber tube per month, in each configuration, in Almeria (Alm) and Berlin (Ber), for the basic dimensions. Figs. 4 and 5 shows, for each configuration,

different cases have been considered, changing the value of the following parameters: mirror length (L_M), receiver height (f), and mirror width (W). The influence of these parameters is evaluated calculating, in percentage terms of the basic dimensions (see Table 3), the change in the monthly energy absorbed by the absorber tube.

4.1.1. Variation of L_M

In configuration C_1 , the influence of increasing L_M is almost nil in the winter months because the negative declination causes reflected rays in this extra length not to reach the absorber tube in almost no time of any day. The length and position of the absorber tube remain constant and they are optimized so that end losses are minimized throughout the year [6]. In winter, the center of the illuminated zone is quite displaced (up to 3.5 m to the right from the center of the mirrors) and this motivates the previous effect. However, in summer with positive declination, the gain is up to 10%, because now the center of the illuminated zone is less displaced (1 m to the right from the center of the mirrors). All these data can be consulted in Fig. 8 [6].

On the contrary, in configurations C_2 and C_3 , when the mirrors are inclined an angle equal to the latitude, this effect is reversed. For example, referring to configuration C_3 , in summer the illuminated zone is displaced 1.5 m to the left from the center of the mirrors, so that the gain is still around 10%. But this gain rises to 25% in winter, because the displacement is much smaller (about half) and then those rays reflected by the extra part can reach the absorber tube. The reasoning is similar for the case of a decrease in the parameter.

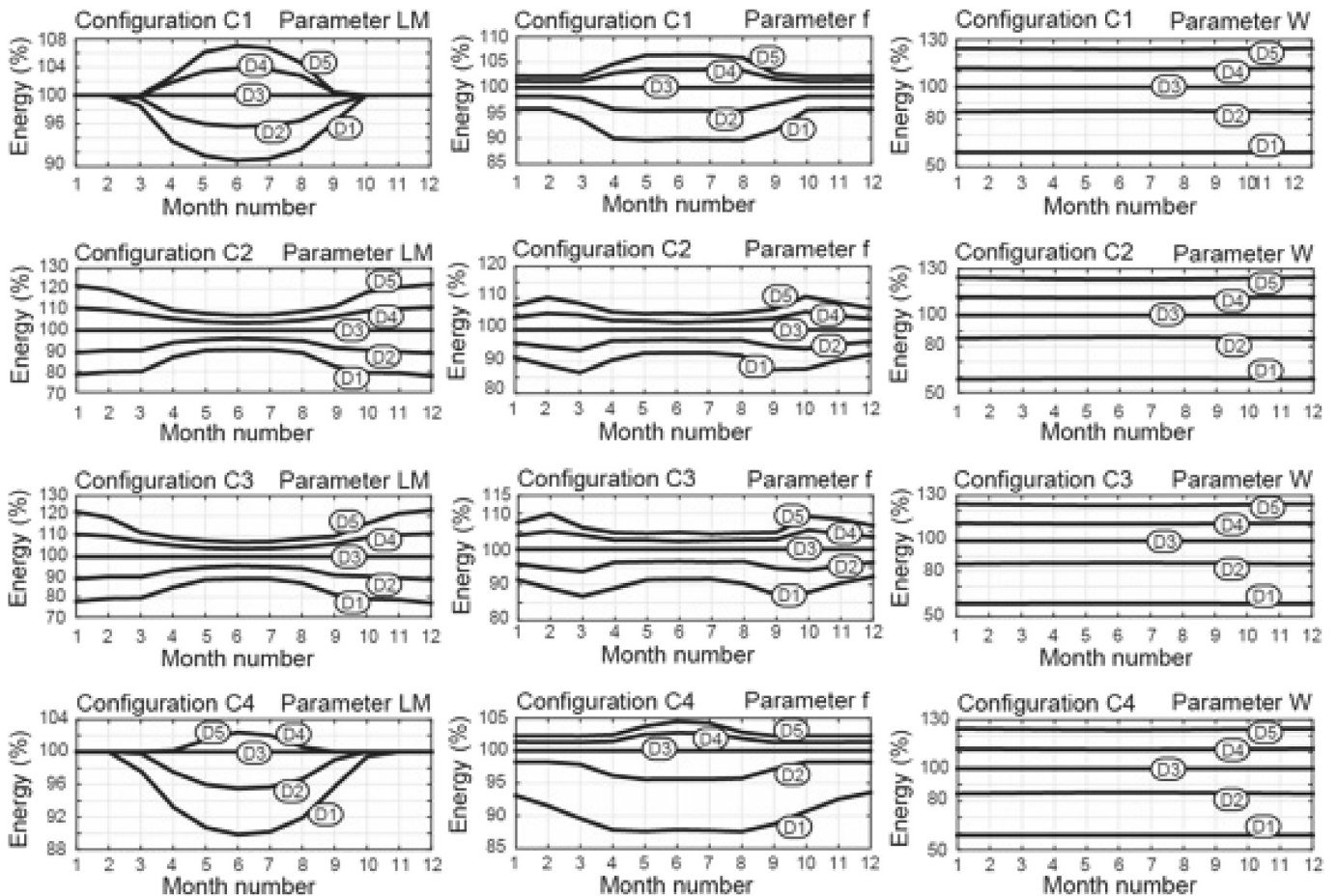


Fig. 4. Monthly energy as a function of the f , L_M and W in Almeria.

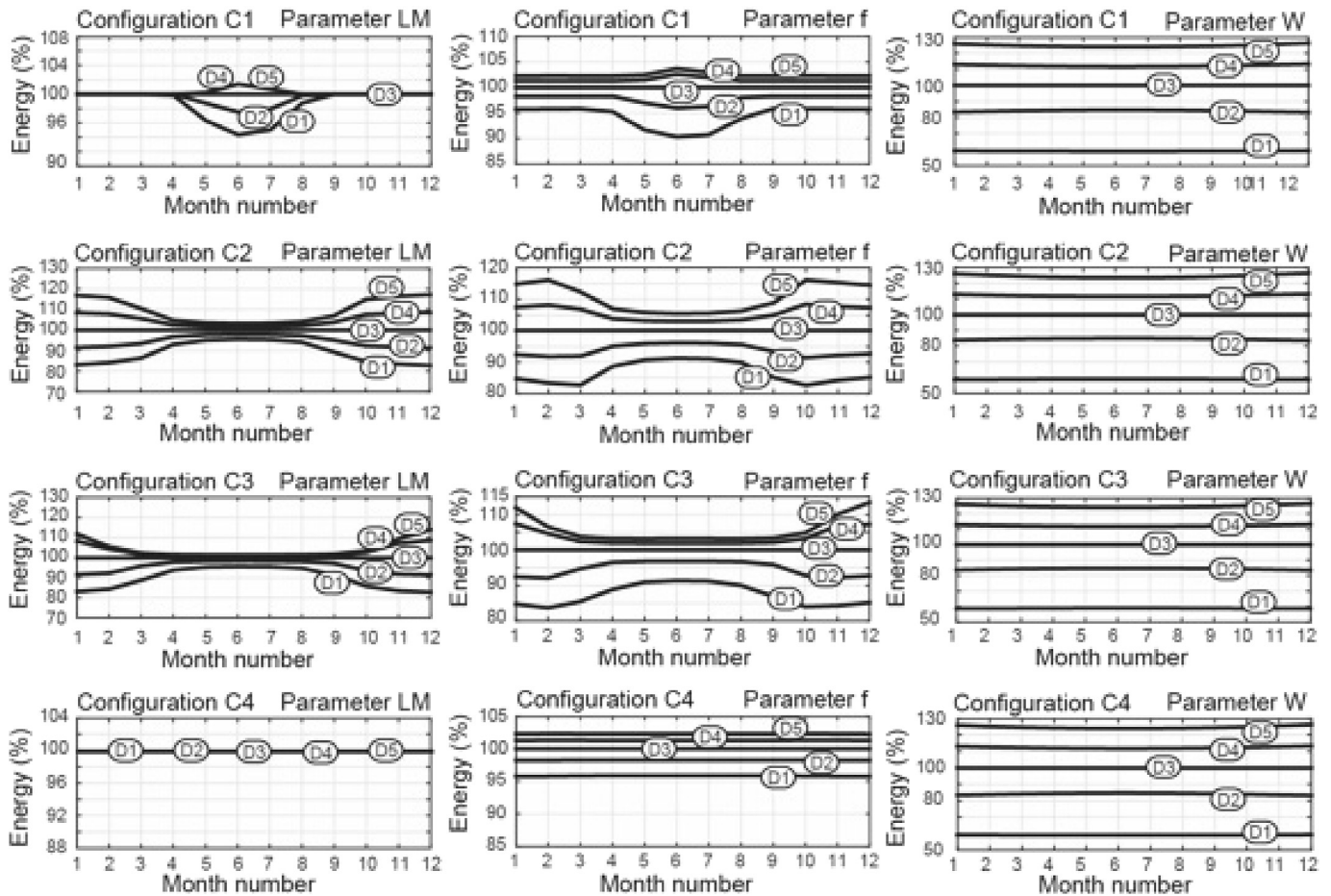


Fig. 5. Monthly energy as a function of the f , L_M and W in Berlin.

In configuration C_4 , the behaviour is similar to configuration C_1 , since the illuminated zone follows an analogous pattern. In addition, due to the small optimum size of the absorber tube ($L_{abs} = 1.217 \text{ m}$), the variation of L_M has no influence.

In Almeria, in configurations C_1 and C_4 the influence of the mirror length is greater in summer. In contrast, in configurations C_2 and C_3 the influence is greater in winter.

4.1.2. Variation of f

When analyzing the increase of f we must take into account that there are two factors that will influence the reflection of the rays and therefore the energy absorbed. First, the effect of the position and length of the absorber tube is similar to that already mentioned above when analyzing the influence of L_M , and for this reason the reader can observe the same general tendency with respect to the summer and winter months. Secondly, we must also consider the cosine factor. It is known that this factor, present in IAF_i calculation (eq (6)), has a great influence on the energy produced. Moreover, in the equinoxes the declination is null, resulting, at noon, in rays perpendicular to the mirrors when their angle is equal to the latitude. Therefore, the results in configurations C_2 and C_3 , are as expected: as the days of the equinox approach, the cosine factor improves and hence the local maximums in absorbed energy on the general trend marked by the influence of the position of the absorber tube. This effect does not appear in configuration C_1 because here the surfaces remain horizontal.

In Almeria, configuration C_4 follows a pattern similar to configuration C_1 . In Berlin, due to latitude, the variation is constant

throughout the year.

In Almeria, in configurations C_2 and C_3 the influence of the receiver height is greater in equinoxes, while in configurations C_1 and C_4 the influence is greater in summer.

4.1.3. Variation of W

The influence of W is constant throughout the year, since, from the transversal point of view, the solar movement throughout the year does not change. In addition, the increase in W has less influence than its decrease. The reason for this behaviour is found in the formulas used to calculate Q . An analysis of these equations shows that IAF_i (eq (6)) includes the parameter A , common to all the mirrors, and the parameter B_i which is different for each mirror. Moreover, A_{effi} includes L_{ai} , the length of the circumference illuminated on the absorber tube by the i -th mirror, where W_{ai} (eq (1)) depends on each mirror.

The increase in W causes an increase in A_{effi} (eq (8)). But the mirrors are then further away from the center of the SSLFR, which results in higher θ_i values that make IAF_i smaller and, therefore, the gain of Q is reduced. However, with a decrease in W , the influence of θ_i is lower and the main effect is the decrease in A_{effi} .

4.2. Influence of the parameters on the shading of the absorber tube

In this section we will study the effect of receiver height (f) and mirror width (W) on the shading of the absorber tube. Mirror length (L_M) does not have any influence on shading. The following parameters have been used for this calculation: Almeria (latitude

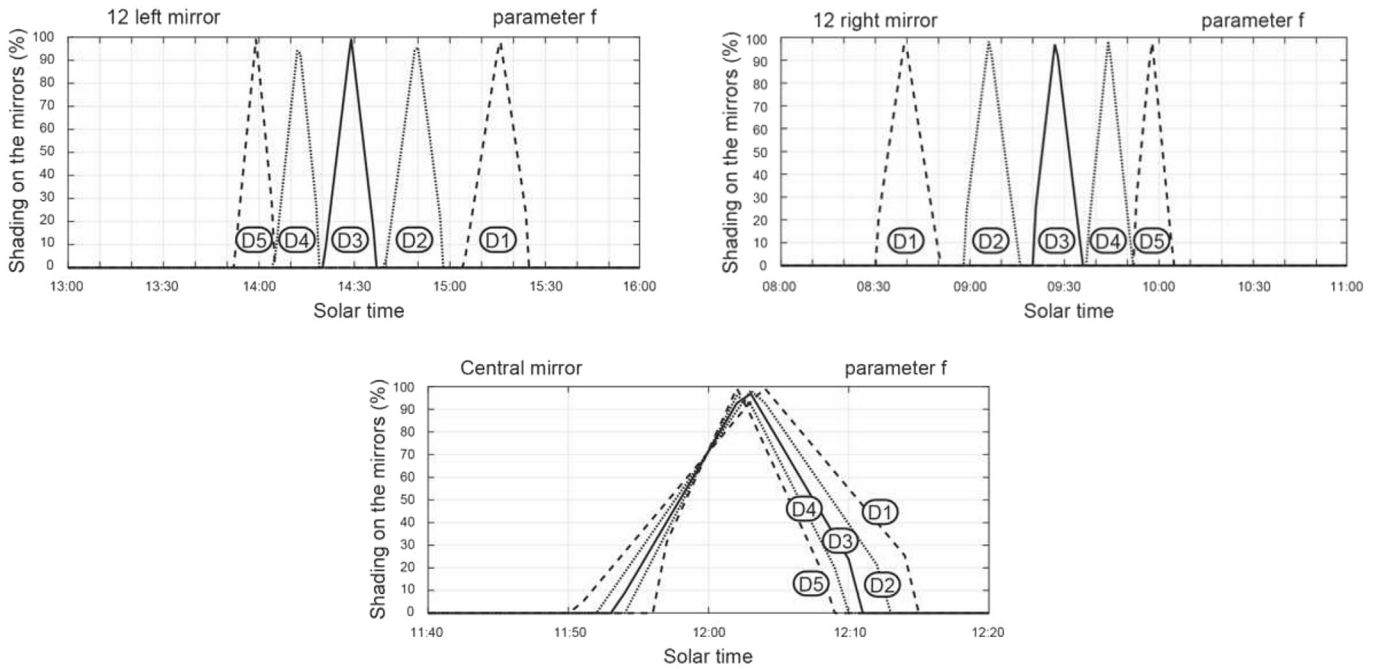


Fig. 6. Shading on the mirrors with variation of receiver height f .

36°50'07"N, longitude 02°24'08"W), 21 June, configuration C₁.

Fig. 6 shows the results of the transversal shading on the mirrors as a function of the solar time and the receiver height (f). As a simplification we show only the shading on 3 mirrors. For example, for $f = 100\%$, the central mirror reaches 96.87% of transversal shading at 12:00, while at 12:11 the transversal shading is 0%. Moreover, the duration of the shading on the mirrors increases with a decrease in f .

Fig. 7 shows the results of the transversal shading on the mirrors

as a function of the solar time and the mirror width (W). The duration of the shading on the mirrors increases with W .

In order to evaluate the total shading on the mirrors, we define a shading index for each day of the year. First we calculate, for each mirror, the shading in percentage terms as a function of time. Then we integrate this function for each mirror and, finally, the shading index is calculated as the ratio between the shaded area over a day and the mirror area.

Fig. 8 shows the value of the shading index as a function of the receiver height (f). As can be seen, the shading index increases with

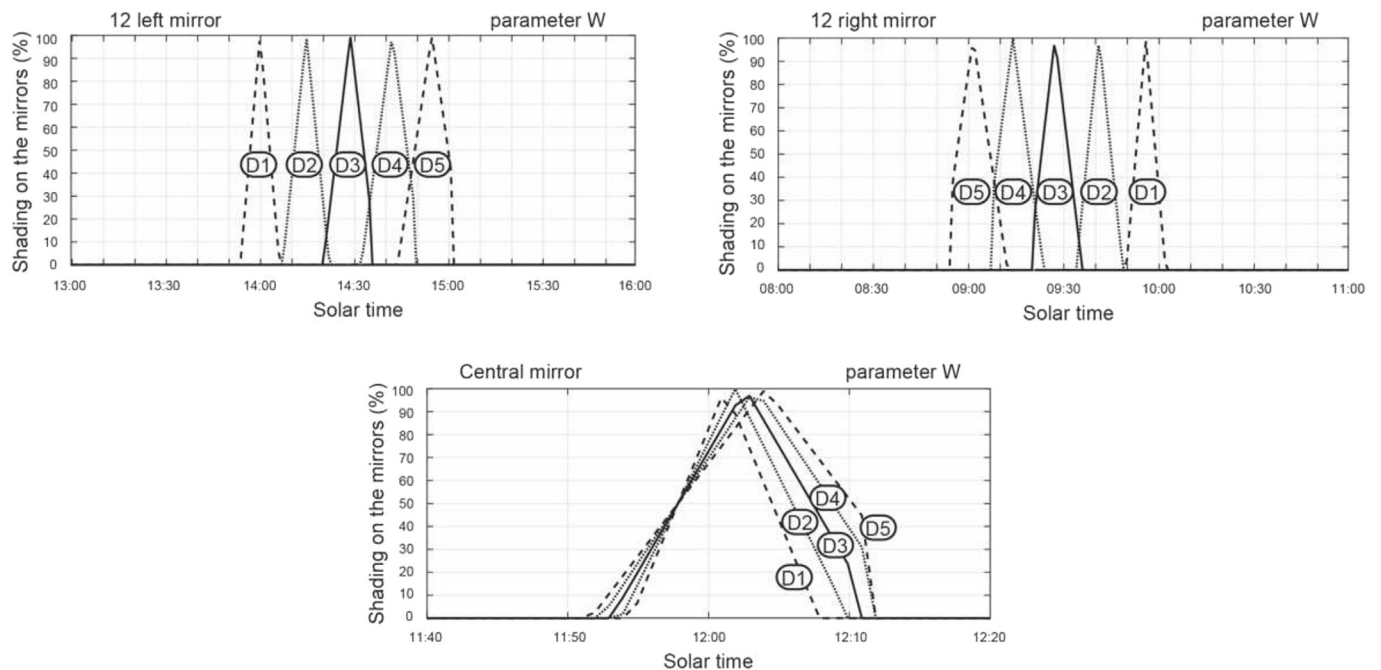


Fig. 7. Shading on the mirrors with variation of mirror width W .

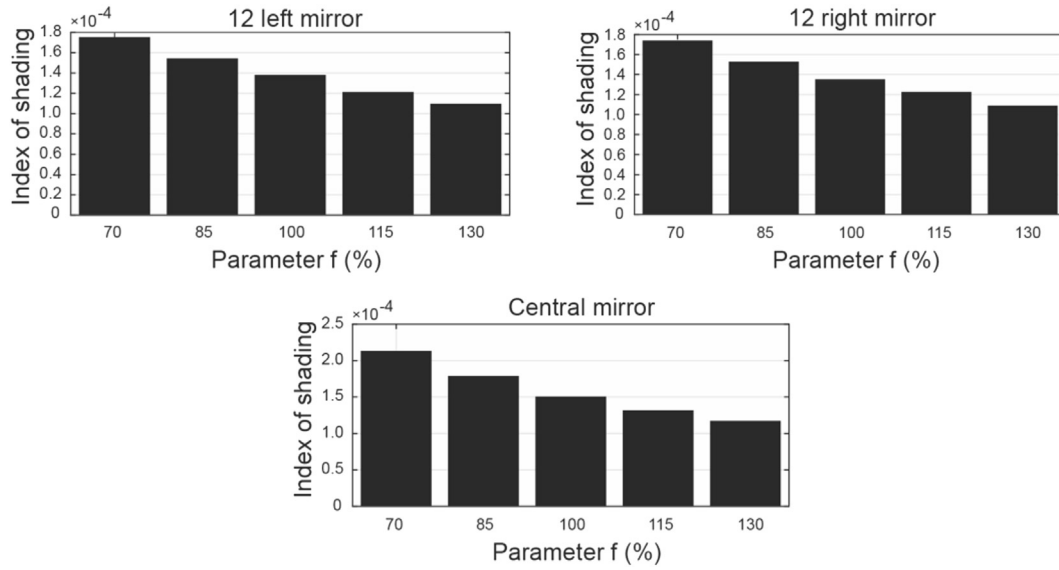


Fig. 8. Shading index with variation of receiver height f .

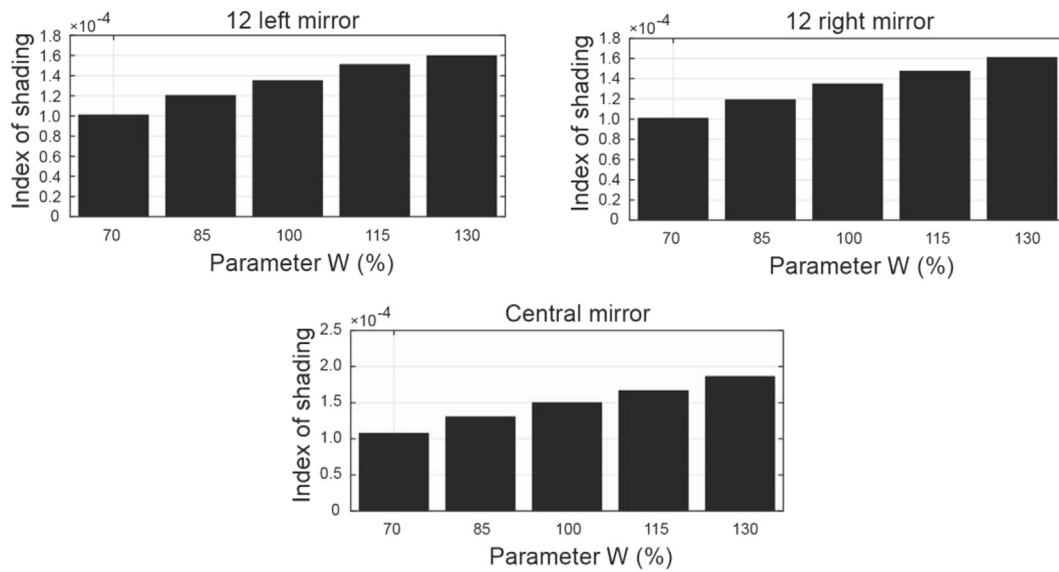


Fig. 9. Shading index with variation of mirror width W .

a decrease in f . Fig. 9 shows the value of the shading index as a function of the mirror width (W). As can be seen, the shading index increases with W . Moreover, the receiver height has a somewhat stronger influence on shading than the mirror width.

4.3. Sensitivity analysis of the parameters

In order to evaluate the importance of the parameters f , L_M and W , a sensitivity analysis was carried out. This analysis evaluates, for each configuration, the influence of one parameter at a time while keeping the others fixed (one-at-a-time method), by using normalized sensitivity coefficients (NSCs) (see Ref. [29]). The NSCs for a particular independent variable can be calculated from the partial derivative of the dependent variable with respect to the independent variable (see Ref. [15], using the equation:

$$NSC_i = \frac{\partial Y}{\partial X_i} \cdot \left(\frac{X_i}{Y} \right) \quad (14)$$

where $\frac{\partial Y}{\partial X_i}$ is the partial derivative of the dependent variable, Y , with respect to the independent variable X_i . $\left(\frac{X_i}{Y} \right)$ is introduced to normalize the coefficient by removing the effects of units. For each configuration, the maximum power output is considered to be the function Y and X_i are the parameters f , L_M and W . The results of the sensitivity analysis are shown in Table 5.

As shown in Table 5, the parameter with the highest NSC is W , which is also practically constant throughout the year, for the four configurations. As regards L_M , its greatest influence takes place in the months of reduced solar irradiance, except for configuration C_1

Table 5
Normalized sensitivity analysis results in Almeria.

| Month | f | | | | L_M | | | | W | | | |
|-------|-------|-------|-------|-------|-------|-------|-------|-------|-------|-------|-------|-------|
| | C_1 | C_2 | C_3 | C_4 | C_1 | C_2 | C_3 | C_4 | C_1 | C_2 | C_3 | C_4 |
| 1 | 0,106 | 0,271 | 0,267 | 0,142 | 0 | 0,717 | 0,738 | 0 | 1,053 | 1,053 | 1,053 | 1,054 |
| 2 | 0,105 | 0,355 | 0,348 | 0,163 | 0 | 0,661 | 0,667 | 0 | 1,050 | 1,046 | 1,048 | 1,050 |
| 3 | 0,135 | 0,366 | 0,325 | 0,191 | 0,022 | 0,579 | 0,549 | 0,033 | 1,047 | 1,037 | 1,041 | 1,046 |
| 4 | 0,243 | 0,244 | 0,248 | 0,229 | 0,155 | 0,379 | 0,408 | 0,120 | 1,043 | 1,029 | 1,035 | 1,042 |
| 5 | 0,275 | 0,206 | 0,213 | 0,261 | 0,245 | 0,295 | 0,320 | 0,180 | 1,041 | 1,025 | 1,031 | 1,039 |
| 6 | 0,274 | 0,203 | 0,211 | 0,269 | 0,271 | 0,272 | 0,299 | 0,214 | 1,039 | 1,023 | 1,029 | 1,037 |
| 7 | 0,275 | 0,201 | 0,208 | 0,267 | 0,261 | 0,280 | 0,306 | 0,200 | 1,040 | 1,024 | 1,030 | 1,038 |
| 8 | 0,268 | 0,212 | 0,229 | 0,244 | 0,204 | 0,332 | 0,362 | 0,142 | 1,042 | 1,027 | 1,034 | 1,040 |
| 9 | 0,180 | 0,312 | 0,287 | 0,207 | 0,070 | 0,487 | 0,485 | 0,064 | 1,044 | 1,033 | 1,039 | 1,044 |
| 10 | 0,108 | 0,382 | 0,359 | 0,174 | 0 | 0,645 | 0,624 | 0,008 | 1,048 | 1,043 | 1,045 | 1,048 |
| 11 | 0,106 | 0,302 | 0,297 | 0,149 | 0 | 0,693 | 0,712 | 0 | 1,052 | 1,051 | 1,052 | 1,053 |
| 12 | 0,106 | 0,242 | 0,239 | 0,136 | 0 | 0,740 | 0,763 | 0 | 1,055 | 1,055 | 1,055 | 1,055 |

and C_4 where the NSC values are lower. Finally, the NSC values of f are around 0.2–0.3 in the four configurations. It should be noted that f is a parameter that does not modify one of the key parameters of design: the mirror field width (M_{fw}). Nevertheless, f has to be taken into account as regards the shading effects between close SSLFRs.

5. Conclusions and future perspectives

This paper addresses the thermal behaviour of a SSLFR, analysing the influence of design parameters in the energy absorbed by the absorber tube.

The variation of the design parameters receiver height, mirror length, and mirror width that describe the transversal and longitudinal design of a SSLFR were analysed, considering the optimal values of the length and longitudinal position of the absorber tube. We have compared the results obtained for different values of the parameters used.

The simulations carried out in this paper provide a detailed analysis of how design parameters affect the performance of a SSLFR, which is essential in order to design an efficient SSLFR. The contributions of this study can be particularly used in the design of SSLFRs to be installed on roofs of buildings, in which the available surface is the most limiting factor. The mathematical model allows to evaluate the influence of design parameters in the area needed to install the reflector.

Numerical simulations show that receiver height, mirror length, and mirror width, have a strong influence on the energy absorbed. Among the analysed cases, a decrease of 30% in the mirror width leads to a maximum decrease in the energy absorbed of almost 59%, an increase of 30% in the receiver height leads to a maximum increase in the energy absorbed of almost 8%, and an increase of 30% in the mirror length leads to a maximum increase in the energy absorbed of almost 24%.

We have also studied the influence of the receiver height and the mirror width on the shading of the absorber tube. We have found that the shading index increases as the receiver height decreases and the mirror width increases. Moreover, the receiver height has a greater impact on shading than the mirror width.

The mirror field area has to be carefully considered, specially if several SSLFRs are to be installed close from one another in a building roof. This parameter depends mainly on the mirror width and the mirror length. The receiver height does not directly affect the mirror field area, however, the shading effects between close SSLFRs need to be analysed.

With regard to possible future works, we are studying the three-movement SSLFR. This design, currently in the process of industrial patent application in Spain, allows the longitudinal movement of

both the primary mirror field and the absorber tube in the N-S direction. Secondly, we are studying the relationship between the roof-related parameters (available roof area, roof form, and roof orientation) and the aspect ratio (AR) of the mirror field area:

$$AR = \frac{2n(W + d) + W}{L_M} \quad (15)$$

Finally, we believe that in order to make better use of the area available on the roofs of urban buildings, it would be very helpful to perform a mathematical optimization of the distribution of SSLFRs.

Acknowledgments

We wish to thank M. F. Fanjul, director of the vocational training school (CIFP-Mantenimiento y Servicios a la Producción) in La Felguera, Asturias, Spain, and the teachers L. Rodríguez and F. Salguero for their work on the (on-going) building of the prototype for the design presented in this paper.

References

- [1] R. Abbas, J. Munoz, J.M. Martínez-Val, Steady-state thermal analysis of an innovative receiver for linear Fresnel reflectors, *Appl. Energy* 92 (2012a) 503–515.
- [2] R. Abbas, M.J. Montes, M. Piera, J.M. Martínez-Val, Solar radiation concentration features in Linear Fresnel Reflector arrays, *Energy Convers. Manag.* 54 (2012b) 133–144.
- [3] R. Abbas, J. Munoz-Anton, M. Valdes, J.M. Martínez-Val, High concentration linear Fresnel reflectors, *Energy Convers. Manag.* 72 (2013) 60–68.
- [4] R. Abbas, J.M. Martínez-Val, Analytic optical design of linear Fresnel collectors with variable widths and shifts of mirrors, *Renew. Energy* 75 (2015) 81–92.
- [5] A. Barbón, N. Barbón, L. Bayón, J.A. Otero, Theoretical elements for the design of a small scale linear Fresnel reflector: frontal and lateral views, *Sol. Energy* 132 (2016a) 188–202.
- [6] A. Barbón, N. Barbón, L. Bayón, J.A. Otero, Optimization of the length and position of the absorber tube in small-scale Linear Fresnel Concentrators, *Renew. Energy* 99 (2016b) 986–995.
- [7] P. Bermejo, F.J. Pino, F. Rosa, Solar absorption cooling plant in Seville, *Sol. Energy* 84 (2010) 1503–1512.
- [8] M. Binotti, G. Manzolini, G. Zhu, An alternative methodology to treat solar radiation data for the optical efficiency estimate of different types of collectors, *Sol. Energy* 110 (2014) 807–817.
- [9] P. Boito, R. Grena, Optimization of the geometry of Fresnel linear collectors, *Sol. Energy* 135 (2016) 479–486.
- [10] G. Cau, D. Cocco, Comparison of medium-size concentrating solar power plants based on parabolic trough and linear Fresnel collectors, *Energy Procedia* 45 (2014) 101–110.
- [11] J.A. Duffie, W.A. Beckman, *Solar Engineering of Thermal Processes*, fourth ed., John Wiley & Sons, New York, 2013.
- [12] Y. Elmaanaoui, D. Saifaoui, Parametric analysis of end loss efficiency in linear Fresnel reflector, in: *Renewable and Sustainable Energy Conference*, 2014, pp. 104–107.
- [13] Directive 2009/28/EC, On the Promotion of the Use of Energy from Renewable Sources, 2009.
- [14] Directive 2010/31/EC, On the Energy Performance of Buildings, 2010.
- [15] D.M. Hamby, *A review of techniques for parameter sensitivity analysis of*

- environmental models, *Environ. Monit. Assess.* 32 (1994) 135–154.
- [16] M. Lin, K. Sumathy, Y.J. Dai, R.Z. Wang, Y. Chen, Experimental and theoretical analysis on a linear Fresnel reflector solar collector prototype with V-shaped cavity receiver, *Appl. Therm. Eng.* 51 (2013) 963–972.
- [17] S.S. Mathur, T.C. Kandpal, B.S. Negi, Optical design and concentration characteristics of linear Fresnel reflector solar concentrators-I. Mirror elements of varying width, *Energy Convers. Manag.* 31 (3) (1991) 205–219.
- [18] S.S. Mathur, T.C. Kandpal, B.S. Negi, Optical design and concentration characteristics of linear Fresnel reflector solar concentrators- II. Mirror elements of equal width, *Energy Convers. Manag.* 31 (3) (1991) 221–232.
- [19] D. Mills, G.L. Morrison, Compact linear Fresnel reflector solar thermal powerplants, *Sol. Energy* 68 (3) (2000) 263–283.
- [20] M.A. Moghimi, K.J. Raig, J.P. Meyer, A novel computational approach to combine the optical and thermal modelling of Linear Fresnel Collectors using the finite volume method, *Sol. Energy* 116 (2015) 407–427.
- [21] M.J. Montes, C. Rubbia, R. Abbas, J.M. Martínez-Val, A comparative analysis of configurations of linear Fresnel collectors for concentrating solar power, *Energy* 73 (2014) 192–203.
- [22] G. Morin, J. Dersch, W. Platzer, M. Eck, A. Häberle, Comparison of linear Fresnel and parabolic trough collector power plants, *Sol. Energy* 86 (2012) 1–12.
- [23] S.K. Natarajan, K.S. Reddy, T.K. Mallick, Heat loss characteristics of trapezoidal cavity receiver for solar linear concentrating system, *Appl. Energy* 93 (2012) 523–531.
- [24] J. Nixon, P. Davies, Cost-exergy optimisation of linear Fresnel reflectors, *Sol. Energy* 86 (2012) 147–156.
- [25] NREL, National Renewable Energy Laboratory, 2017. Available on line at, https://www.nrel.gov/csp/solarpaces/project_detail.cfm/projectID=37.
- [26] F.J. Pino, R. Caro, F. Rosa, J. Guerra, Experimental validation of an optical and thermal model of a linear Fresnel collector system, *Appl. Therm. Eng.* 50 (2013) 1463–1471.
- [27] PVGIS, Joint Research Centre (JRC), 2017. Available on line at, <http://re.jrc.ec.europa.eu/pvgis/apps4/pvest.php>.
- [28] V.M. Sharma, J.K. Nayak, S.B. Kedare, Comparison of line focusing solar concentrator fields considering shading and blocking, *Sol. Energy* 122 (2015) 924–939.
- [29] M.U. Siddiqui, A.F.M. Arif, A.M. Bilton, S. Dubowsky, M. Elshafei, An improved electric circuit model for photovoltaic modules based on sensitivity analysis, *Sol. Energy* 90 (2013) 29–42.
- [30] T. Sultana, G.L. Morrison, G. Rosengarten, Thermal performance of a novel rooftop solar micro-concentrating collector, *Sol. Energy* 86 (2012) 1992–2000.
- [31] T. Sultana, G.L. Morrison, R.A. Taylor, G. Rosengarten, Numerical and experimental study of a solar micro concentrating collector, *Sol. Energy* 112 (2015) 20–29.
- [32] P.-H. Theunissen, W.A. Beckman, Solar transmittance characteristics of evacuated tubular collectors with diffuse back reflectors, *Sol. Energy* 35 (1985) 311–320.
- [33] N. Velázquez, O. García-Valladares, D. Saucedo, R. Beltrán, Numerical simulation of a linear Fresnel reflector concentrator used as direct generator in a solar-GAX cycle, *Energy Convers. Manag.* 51 (2010) 434–445.